19th Australasian Fluid Mechanics Conference
Melbourne, Australia
8-11 December 2014

Entrainment Across a Sharp Density Interface in a Sheared Cavity Flow

N. Williamson[1], M. P. Kirkpatrick[1], S. W. Armfield[1] and S. H. Starner[1]

[1]School of Aerospace, Mechanical and Mechatronic Engineering, The University of Sydney, New South Wales 2006, Australia

Abstract

The turbulent entrainment of fluid across a sharp density interface has been examined experimentally in a purging cavity flow. In the experiments, a long straight cavity with sloped entry and exit boundaries is located in the base of a straight open channel. Saline fluid is entrained from the cavity into the overflow. The entrainment rate and its dependence on geometric parameters and flow properties are of primary interest. This flow is similar to that commonly encountered in Australian inland river systems subjected to saline ground water intrusion.

The cavity geometry has been designed to ensure there is no separation of the overflow in the cavity region with the goal of obtaining a single mode of entrainment, related only to the local interface stability properties rather than to cavity specific mechanisms which have been encountered in most previous experiments. Results are obtained over a Richardson number range $\mathrm{Ri} = 1.0 - 20$ at bulk Reynolds number $\mathrm{Re} = 7100 - 15100$.

Entrainment rate measurements have been made using three independent approaches to ensure the veracity of the data and demonstrate the method's suitability. The results show an extended region where the non-dimensional entrainment rate scales with the local bulk Richardson number $E \sim Ri^{-1.38}$, very close to the scaling obtained empirically by Strang and Fernando [9] for entrainment across a sharp two layer density interface. The result is a strong indication that the flow is dominated by a local shear driven entrainment mechanism at the interface. The results suggest the scaling is only weakly sensitive to the length of the interface, which is varied through the experiments. The result can be used to better delineate between entrainment modes in other cavity geometries.

Introduction

Many of Australia's inland rivers are subject to saline intrusions that occur in deep river pools and are associated with high nutrient levels and low oxygen concentrations, which are hazardous to most riverine life. This issue can be mitigated by environmental release of stored water upstream, which can purge the saline intrusions from the pools. Effective management requires an understanding of these processes so that water is used efficiently with known downstream effects. The flow is also of interest with relation to pollution dispersion in valleys and urban street canyons [7, 1] as well as other geophysical problems including flow in estuaries and ocean trenches.

A schematic representation of the flow setting is provided in figure 1. Fresh water flows in an open channel of depth H over a cavity containing more dense saline water at an initial depth C_0 and length l_C. The saline fluid is entrained into the overflow with entrainment velocity u_e, over time depleting the cavity such that the cavity depth C and interface length L decrease with time while D increases. The rate of this fluid exchange and its underlying mechanism are the subject of this investigation.

Previous studies of low aspect ratio cavities, where $l_c/C_0 \simeq 1-2$ [7, 1], have shown that the flow can be characterised by an interface entrainment mechanism coupled with a turbulent exchange mechanism between the turbulent overflow and the cavity interior. In that geometry the overflow separates from the leading edge of the cavity and circulation within the cavity is significant [7].

Debler and Armfield [3] performed experiments at larger aspect ratios and also varied cavity entry and exit angles to develop a scaling for the purging rate which accounts for interface height. Chu and Baddour [2] examined the flow development of a planar surface jet over a density interface. The authors showed using laboratory experiments that their flow initially expands as a planar wall jet before relaxing to a planar mixing layer flow. Kirkpatrick, Armfield and Williamson [8] showed using Large Eddy Simulation (LES) and the experimental results of Debler and Armfield [3] that the entrainment behaviour in the cavity flow can be similarly delineated between these two distinct regions. As the overflow initially expands over the cavity, entrainment scales with the length and velocity scales of a planar surface jet (region 1) with $E \sim \mathrm{Ri}_b^{-1}$ while further along the cavity in the planar mixing layer (region 2) the authors found $E \sim \mathrm{Ri}_b^n$ where $n \simeq -1$ is a constant. Implicit in this model is a switch to local length scales D, U which account for variation in interface height within the cavity. The authors found improved correlation among experimental data sets using this two region flow structure.

Most previous cavity flow experiments and simulations have contained large regions of upstream flow separation which significantly increases overall mixing in the cavity, leading to predominantly region 1 mode of entrainment. This has made it difficult to test scaling relationships for entrainment in the two regions leaving two significant outstanding questions. Firstly, does the region 2 behaviour, as it occurs in the cavity setting, differ from the entrainment across a sheared density interface in other configurations? Secondly, does the length of the mixing layer in the cavity modify the average entrainment rates? In an attempt to answer these questions, a new laboratory rig has been designed to obtain predominately the planar mixing layer regime within the cavity flow setting, and to allow for a very long interface development length.

Problem Description

The non-dimensional entrainment rate $E = u_e/U$ is expected to contain a functional dependence

$$E = f(L, D, C, H, \Delta b, \nu, \kappa, U), \tag{1}$$

where the buoyancy difference $\Delta b = g\Delta\rho/\rho_0$, κ is the molecular diffusivity of salinity and ν is the kinematic viscosity. The local time varying geometric properties L, D are adopted as the functional outer flow length scales. Strang and Fernando [10] found the shear layer thickness at a shear density interface correlates with $\delta_s \sim D$, supporting this assumption in the planar mixing layer regime. In non-dimensional form this function set can be reduced to

$$E = f(\mathrm{Ri}_b, \mathrm{Re}, \mathrm{Pe}, \mathrm{Sc}, A), \tag{2}$$

where A contains the relevant geometric aspect ratios, which may include $A = [L/D, L/H, D/H, \theta_1, \theta_2]$ and $\mathrm{Re} = U_0 H/\nu$,

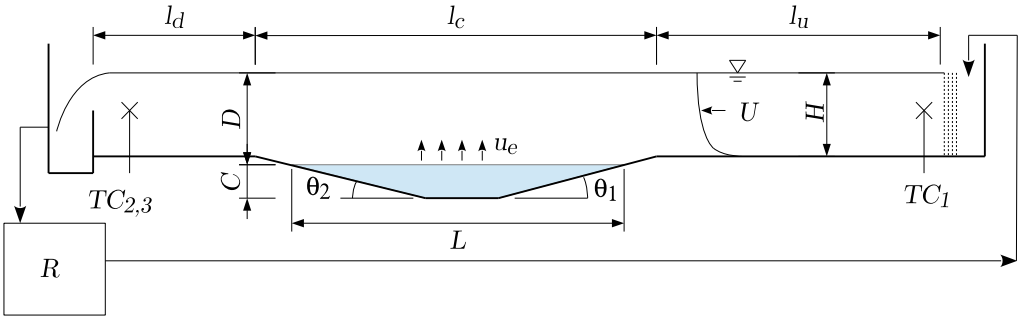

Figure 1: Schematic representation of the flow and experimental apparatus. Flow is from right to left and re-circulates via a reservoir.

$Sc = \nu/\kappa$, $Pe = U_0 H/\kappa = \mathrm{Re}\,Sc$ and $\mathrm{Ri}_b = \Delta b D/U^2$ noting that the non-dimensional groups are also time varying within each experiment in response to D varying with $U = U_0 H/D$ from continuity. The fluid property $Sc \simeq 700$ for saline water solutions gives $\mathrm{Pe} \simeq 10^7$.

We test these dependencies by varying L/D within each experiment by allowing D to increase and also by physically reducing the initial l_c by changing the cavity inserts. We vary the Reynolds number over $\mathrm{Re} = 7100 - 15100$.

Experiments

Our laboratory rig is illustrated in figure 1. Water is pumped to the plenum box at the start of the channel after which it flows through flow conditioners and then along the channel over the cavity insert to an overflow weir at the end and into a $0.9\,\mathrm{m}^3$ storage reservoir. The reservoir level is maintained at $0.55\,\mathrm{m}^3$ capacity and is stirred continuously with two submersible pumps with 800L/min flow capacity to maintain a homogeneous but time varying reservoir salinity. The channel and cavity is initially filled with fresh water and then additional saline water is fed into the cavity base, displacing the fresh water, so a sharp two layer saline stratification is achieved. The purging flow is initiated by turning on the fresh water pump.

The rig has a channel width $B = 0.50\,\mathrm{m}$, cavity length $l_c = 1.6 - 2.1\,\mathrm{m}$, upstream development length $l_u = 2.5\,\mathrm{m}$, downstream length $l_d = 1.4\,\mathrm{m}$, cavity entry and exit angles $\theta_1 = 6.2^\circ$ and $\theta_2 = 8.0^\circ$ respectively. The channel depth at the entrance to the cavity, the cavity depth and overflow height are constant at $C_0 = D_0 = H = 0.1\,\mathrm{m}$.

The majority of the experiments were performed at $U_0 = 0.113\,\mathrm{m/s}$ giving $\mathrm{Re} = 11300$ with additional runs at $0.071\,\mathrm{m/s}$, and $0.151\,\mathrm{m/s}$ giving $\mathrm{Re} = 7100$, and $\mathrm{Re} = 15100$ respectively. The Froude number for the free surface channel flow is $Fr = 0.07 - 0.15$, well within the sub-critical flow regime.

The initial $\mathrm{Ri}_0 = \Delta b U_0/H = 0.25 - 3.6$, with density difference $\Delta\rho/\rho_0 = 0.0013 - 0.047$ where $\Delta\rho = \rho_c - \rho_0$ and ρ_c and ρ_0 are the density of the cavity solution and fresh overflow respectively. The density difference is obtained by varying the cavity fluid salinity (σ) over the range, $\sigma = 2.3 - 72.3\,\mathrm{g\,NaCl/L}$.

The cavity is initially filled with saline fluid to $C = C_0 = 0.1\,\mathrm{m}$. The initial start-up of the flow sets up a wave in the cavity interface and 'splashes' out a volume of cavity fluid [3, 5]. The initial splash and cavity seiche is reduced by initiating the flow with a 120 second ramped start-up. Data is only retained once the transient start up effects have dissipated, so C is necessarily less than C_0. Additionally, the experiments are suspended when the interface depth is reduced to $C = 0.018\,\mathrm{m}$ to limit interaction between the density interface and the base of the cavity. With these limitations the range of conditions experienced in the flow covers $Ri_b = 1.1 - 19$, as illustrated in figure 2. The flow in the real river system is expected to have parameters in the range $\mathrm{Re} > 2 \times 10^5$ and $\mathrm{Ri}_b = 10 - 150$.

Entrainment Measurements

During the experiments the cavity is illuminated by stage lights behind a diffusive screen. A non-buoyant food dye is used as a passive tracer in the saline fluid for visualisation purposes. A camera, which views the cavity from a side orientation, records images of the 200 mm square region at the center of the cavity at 1Hz. The stored images are then used to obtain the time varying interface depth C. The images are filtered horizontally to remove small scale surface waves. The change in image intensity between the fresh and saline fluid allows the interface to be located and the flow depth D, interface length L, interface area LB and local overflow velocity $U = U_0 H/D$ to be obtained.

The rig is also instrumented with three temperature/conductivity probes at the upstream TC_1 location and downstream $TC_{2,3}$ location indicated in figure 1. The flow in the downstream straight section is homogenised by small turbulence promoters in the exit section before the $TC_{2,3}$ location. The two downstream probes are fast response temperature conductivity probes (model 125 MicroScale (MSCTI) made by Precision Measurement Engineering) which simultaneously record the flow conductivity and temperature. The upstream probe is a Kenek MK-103 (Keisoku Giken Co. Ltd). All probes are logged at 100Hz through a NI cDAQ board to a PC. All probes are calibrated with known saline solutions before and after each experiment with a third order regression fit used to obtain the solution salinity, σ. The correction for temperature effects of conductivity are made using the linear temperature conductivity relations from Hewitt [6]. The MSCTII probes have a linear voltage response to conductivity from $0.5 - 800\,\mathrm{mS/cm}$ which leads to a lower measurement limit at $18^\circ\,\mathrm{C}$ of approximately $0.3\,\mathrm{g\,NaCl/L}$. The entrainment of saline fluid leads to a change in salinity of between 0.02-1.1 g NaCl/L across the cavity through the experiments. The recirculating flow increases in salinity with entrainment from the cavity so the density difference $\Delta\rho/\rho_0$ decreases slowly with time. This effect on the time varying Ri_b is calculated. Salinity and D(t) measurements are filtered over a period of 20 s to obtain smooth time-series for calculation of entrainment.

The entrainment velocity u_e has been been obtained indirectly using three independent approaches. The first measure is obtained using the change in interface depth as,

$$u_{e,\delta h} = dV/dt(1/LB) \tag{3}$$

where V is the remaining volume of saline solution in the cavity. This method has been used successfully in previous studies [3, 7]. With the data collected in the present work V can only be estimated assuming constant interface depth across the cavity leading to a systematic error in $u_{e,\delta h}$ that we estimate to be $<$ 10% for $C < 0.7C_0$.

A second measurement approach takes the difference in salinity recorded across the cavity σ_1 and $\sigma_{2,3}$ at probes TC_1 and $TC_{2,3}$. The change in salinity experienced by a volume of fluid advected from location 1 to $2,3$ can be obtained by a temporal shift in the time-series $\sigma_1(t)$ and $\sigma_{2,3}(t)$ by the advection time $\tau = \int_0^L dx/U(x)$. This is implemented as a shift in both upstream and downstream signals to the cavity center location to be consistent with our $D(t)$ and $L(t)$ measurements. The entrainment rate can then be obtained from

$$u_{e,\delta\sigma} = U_0 BH[\sigma_{2,3}(t-\tau_{2,3}) - \sigma_1(t+\tau_1)]/(BL(t)\sigma_c), \quad (4)$$

where τ_1 and $\tau_{2,3}$ are the advection time between the center of the cavity and the probe locations. A third measure of entrainment is also obtained by the rate of change of salinity in the $\sigma_1(t)$ series. The recirculating flow stream increases in salinity which allows the entrainment rate to be obtained from equation (4) but instead using an estimate for the downstream salinity $\sigma^*_{2,3}(t)$ obtained from,

$$\sigma^*_{2,3} = \frac{d\sigma_r}{dt}\frac{1}{\alpha} + \sigma_r, \quad (5)$$

where $\sigma_r = \sigma_1(t-\tau_r)$ and τ_r is the temporal shift between reservoir and the probe at location 1. As the homogeneity of the reservoir becomes more complete $\alpha \to V_r/Q$ where V_r is the reservoir volume and Q is the flow rate. We obtain τ_r and α directly from flow for every Q and V_r setting used. Both instantaneous and continuous releases of fluid from the cavity and at the entrance to the reservoir are used to determine the veracity of the method. The method simplifies the rig instrumentation which is an advantage when performing other types of experiments such as simultaneous PIV/PLIF work. Unless otherwise stated the results presented are obtained with equation (4) with (5). Measurements obtained from method 1 and 2 are consistent with variation within expected experimental error. The findings presented are independent of the method used.

Results

The entrainment rate results for all the data collected is presented in figure 3 with the three Reynolds number ranges indicated. We obtain a regression fit of $E = C\,\mathrm{Ri}^n$ with $n = -1.38$ and $C = 0.0023 \pm 0.0007$ for the more extensive $\mathrm{Re} = 11300$ results. Data obtained using equation (3) for the same experiments gives $n = -1.35$ and $C = 0.0022 \pm 0.0007$ (data not shown). Within the data presented there is no apparent sensitivity to Reynolds number.

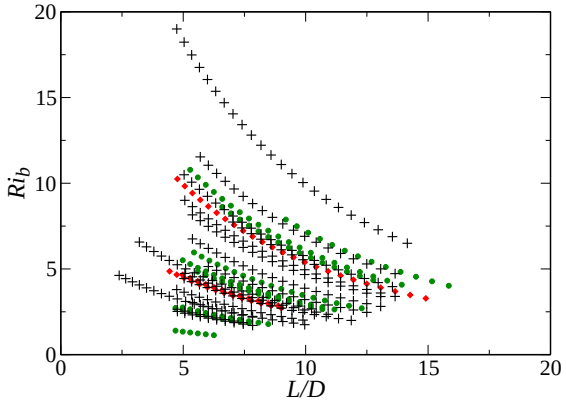

Figure 2: Experiments performed with instantaneous realisations of time varying Ri and flow aspect ratio L/D. Black symbols: $\mathrm{Re} = 11300$, Red symbols $\mathrm{Re} = 15100$ and Green symbols $\mathrm{Re} = 7100$.

Strang and Fernando [10] made measurements of entrainment across a sheared density interface in an Odell–Kovasznay type re-circulating water channel. They observed two high Richardson number regimes of behaviour. In their regime 2 over $\mathrm{Ri}_b = 1.5-5$ they observed $E \simeq CRi_b^n$ where $C_2 \simeq 0.22 \pm 0.11$ and $n \simeq -2.63 \pm 0.45$. At higher Richardson number, in their regime 3 over $\mathrm{Ri}_b = 5-20$ they found $C_3 \simeq 0.02 \pm 0.01$ and $n \simeq -1.3 \pm 0.15$. Both these relationships are presented in figure 3. Our exponent $n = -1.38$ lies within the the range of values they report for their regime 3 but our constant C is approximately an order of magnitude smaller and we observe this scaling holds down to $\mathrm{Ri}_b \simeq 1$.

The consistency among the exponent values between the studies suggests that similar mechanisms may be present, that is in both flows entrainment is driven by shear driven effects at the interface rather than cavity related mechanisms. Shear driven entrainment at a density interface can be correlated with the local gradient Richardson number Ri_g [4]. Strang and Fernando [10] observed the relationship $\mathrm{Ri}_g \sim \mathrm{Ri}_b^2$ in their experiments. We conjecture that the large difference between the coefficient C in the two studies may be explained by a different constant of proportionality in this relationship. We note that Ri_B is a global parameter but local conditions vary along the interface as the mixing layer develops. An important difference between our study and the configuration in [10] is the finite nature of the interface length. At the entrance to our cavity the mixing layer thickness δ_b is expected to be close to zero, so in general we expect the cavity flow to have a sharper density interface than a re-circulating water channel for the same Ri_b.

We have examined the sensitivity of the entrainment to geometric properties in figure 4. Here we have binned the results into bands of L/D, D/H, L/H and plotted the arithmetic mean of the correlation coefficient C for the data within each bin. The range of data is indicated by the bars in the figure. It is clear the variation in the mean C is within the scatter of the data over all L/D, D/H, L/H plotted. There is a slight reduction in C at large L/D, L/H or small D/H. The data for the $l_c = 2.1$ and $l_c = 1.6$ experiments are highlighted separately. Plotted against L/D and L/H the mean results lie within scatter in both data sets. Plotted against D/H there is more significant separation at small D/H suggesting that the entrainment rate may be weakly sensitive to interface length.

The relative insensitivity of our results to interface length suggests that the development of the mixing layer above the interface occurs at a length scale much larger than $L/D = 18$ and that a single bulk Richardson number is an effective parameter to characterise the flow along the entire length of the interface up to this limit.

Acknowledgements

The authors acknowledge the support of the Australian Research Council under grant DP110103417.

References

[1] Baratian-Ghorghi, Z. and Kaye, N. B., Modeling the purging of dense fluid from a street canyon driven by an interfacial mixing flow and skimming flow, *Physics of Fluids*,

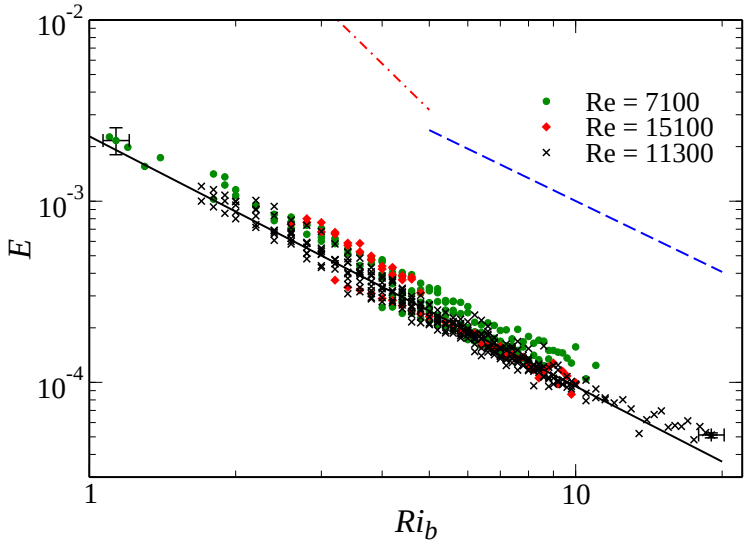

Figure 3: Entrainment rate $E = u_e/U$ for all data with Re = 11300 (black symbols), Re = 7100 (green symbols) and Re = 15100 (red symbols). Solid black line indicates $E = CRi^n$ where $C = 0.0023$ and $n = -1.38$. Data from [9] are given by dashed-dotted red line ($C = 0.22$,$n = -2.63$) and dashed blue line ($C = 0.02$,$n = -1.3$).

25, 2013, 076603.

[2] Chu, V. H. and Baddour, R. E., Turbulent gravity-stratified shear flows, *Journal of Fluid Mechanics*, **138**, 1984, 353–378.

[3] Debler, W. and Armfield, S. W., The purging of saline water from rectangular and trapezoidal cavities by an overflow of turbulent sweet water, *Journal of Hydraulic Research*, **35**, 1997, 43–62.

[4] Fernando, H. J. S., Turbulent patches in a stratified shear flow, *Physics of Fluids*, **15**, 2003, 3164–3169.

[5] Gillam, N. L., Armfield, S. W. and Kirkpatrick, M. P., Influence of a channel bend on the purging of saline fluid from a cavity by an overflow of fresh water, *ANZIAM Journal*, **50**, 2009, C990—C1003.

[6] Hewitt, G. F., Tables of the resistivity of aqueous sodium chloride solutions, Technical Report AERE-R-3497, United Kingdom Atomic Energy Authority. Research Group. Atomic Energy Research Establishment, Harwell, Berks, England, 1960.

[7] Kirkpatrick, M. P. and Armfield, S. W., Experimental and large eddy simulation results for the purging of salt water from a cavity by an overflow of fresh water, *International Journal of Heat and Mass Transfer*, **48**, 2005, 341–359.

[8] Kirkpatrick, M. P., Armfield, S. W. and Williamson, N., Shear driven purging of negatively buoyant fluid from trapezoidal depressions and cavities, *Physics of Fluids*, **24**, 2012, 025106.

[9] Strang, E. J. and Fernando, H. J. S., Entrainment and mixing in stratified shear flows, *Journal of Fluid Mechanics*, **428**, 2001, 349–386.

[10] Strang, E. J. and Fernando, H. J. S., Shear-induced mixing and transport from a rectangular cavity, *Journal of Fluid Mechanics*, **520**, 2004, 23–49.

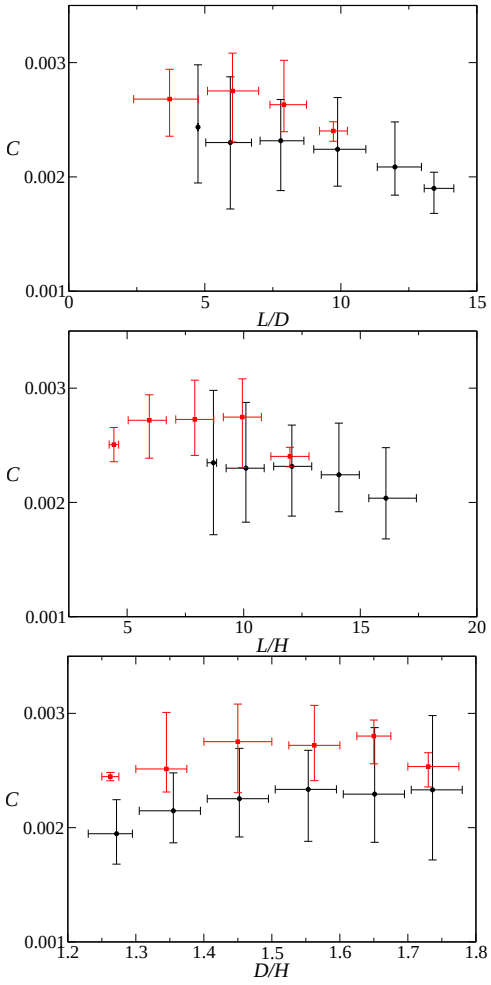

Figure 4: Correlation coefficient $C = E\,\mathrm{Ri}^{1.38}$ with flow aspect ratio L/D, L/H and D/H for $l_c = 2.1$ (black symbols) and $l_c = 1.6$(red symbols) for Re = 11300. Mean values plotted with bars giving range of data.